Molecular Modeling in Support of CO$_2$ Sequestration and Enhanced Oil Recovery

Louise J. Criscenti and Jacquelyn Bracco

Sandia National Laboratories

Molecular Modeling in Support of CO$_2$ Sequestration and Enhanced Oil Recovery

Louise J. Criscenti
Geochemistry Department
Sandia National Laboratories
P.O. Box 5800 MS 0754
Albuquerque, New Mexico 87185

and

Jacquelyn Bracco
School of Earth and Atmospheric Sciences
Georgia Institute of Technology
Atlanta, Georgia 30332

Abstract

Classical molecular dynamics simulations were used to investigate the formation of water droplets on two kaolinite surfaces: the gibbsite-like surface which is hydrophilic and the silica surface which is hydrophobic. Two methods for calculating contact angles were investigated in detail. The method of Giovambattista et al. was successful in calculating contact angles on both surfaces that compare well to the experimental data available. This is the first time that contact angles have been calculated for kaolinite surfaces from molecular simulations. This preliminary study provides the groundwork for investigating contact angles for more complex systems involving multiple fluids (water, CO$_2$, oil) in contact with different minerals in the subsurface environment.

Acknowledgments

We want to thank Christopher Daub, a Postdoctoral Associate at Virginia Commonwealth University for sharing his insight on calculating contact angles from LAMMPS trajectory data and providing his FORTRAN code for making these calculations. We learned a great deal from his letter giving us an overview of the state of the art, and we used his code to educate us on the binning process for the liquid drop.

Contents

Figures

Tables

1. Introduction

Storage of carbon dioxide in sedimentary basins is a proposed method of sequestration for CO_2 emissions from power plants. A commonly proposed method of storage compresses CO_2 to the liquid form prior to or during injection into a basin. Liquid CO_2 is then converted to supercritical CO_2 with increasing depth. One proposed scenario is that CO_2 would be injected into a porous sandstone reservoir, which is either partially or fully saturated with groundwater, or a combination of groundwater and oil, and is overlain by an impermeable shale caprock. Because CO_2 injected into a porous media will replace present-day pore fluids including water, oil, and air, understanding the relative wettability of the sandstone and shale to these fluids is critical to predicting the outcome of CO_2 sequestration. If water and oil adhere to sedimentary rocks better than CO_2, then CO_2 will flow more readily through the middle of the pores, and is likely to migrate back to the earth surface through rock fractures. If CO_2 adheres strongly to mineral surfaces, then it will be more likely to remain sequestered over long periods of time.

The relative wettability of different minerals found in the subsurface environment (e.g., quartz, kaolinite and smectite) can be investigated through large-scale molecular dynamics simulations. The wettability of a solid surface is often characterized by measuring the contact angle formed between a liquid, its vapor and a solid surface. A contact angle less than 90 degrees, indicates the surface is hydrophilic and wetting is favorable. A contact angle greater than 90 degrees indicates the surface is hydrophobic and wetting is not favorable. Contact angles can also form between two fluids such as supercritical CO_2 and water or supercritical CO_2 and oil. In this report, we develop an approach to calculate contact angles from classical molecular dynamics using kaolinite as a representative clay mineral found in sedimentary basins and water as a fluid. To our knowledge, this is the first time that contact angles have been calculated for a mineral surface other that silica using molecular dynamics simulations. This approach will be useful in the future to investigate the wettability of quartz and different clay minerals to oil, supercritical CO_2, and water.

2. Background

The wetting behavior of a liquid droplet on a surface exposed to vapor is defined by the Young equation:

$$\gamma_{12} + \gamma_2 cos\theta_0 = \gamma_1 \tag{2.1}$$

where γ_1 and γ_2 are the free energy changes when the surface areas of mediums 1 and 2 are increased by a unit area respectively. When two immiscible liquids 1 and 2 are in contact, the free energy change in expanding their "interfacial" area by one unit area is known as their interfacial energy or interfacial tension γ_{12}. This equation can be generalized to calculate the interfacial energies and contact angle between two liquids and a solid surface. The contact angle at equilibrium, θ_0, is a macroscopic thermodynamic property, independent of the nature of the forces between the molecules as long as these are of shorter range than the dimensions of the droplet (Israelachvili, 1992).

Wetting is commonly characterized by the contact angle, that is, the angle at which the tangent to the liquid-liquid interface intersects the solid. If this angle is different from 0 or pi, it is said that the solid is partially wetted by the liquids. Several groups have calculated contact angles from large-scale molecular dynamics simulations. However, this is a relatively new area of research and no consistent approach to making these calculations has been established.

Hautman and Klein (1991) used molecular dynamics calculations to investigate wetting phenomena on a microscopic length scale. Their model system consisted of 90 water molecules on either hydrophobic or hydrophilic surfaces formed by monolayers of long-chain molecules with terminal $-CH_3$ or $-OH$ groups. They calculated the microscopic wetting angle by comparing the average height of the center of mass of the water cluster to that of an ideal sessile drop in the shape of a sphere intersecting a surface plane. The angle of intersection between the surface of the sphere and the plane defines a contact angle for the droplet. They concluded that the results were similar to the corresponding macroscopic wetting phenomena and that simulations on the order of 10^3 particles might be sufficient to predict macroscopic properties such as the wetting contact angle.

Fan and Cagin (1995) expanded on the approach of Hautman and Klein. They studied the wetting of crystal surfaces of polyethylene, polytetrafluoroethylene, and polyethylene terephthalate by water and methylene iodide. They pointed out that the conventional contact angle measured experimentally becomes ill-defined at the molecular level (Figure 2.1). Therefore, one goal of their study is to develop a general approach to interpreting the contact angle from a microscopic configuration that can be compared successfully to experiment. They calculate the *instantaneous* contact angle from the microscopic structures of the droplet and the
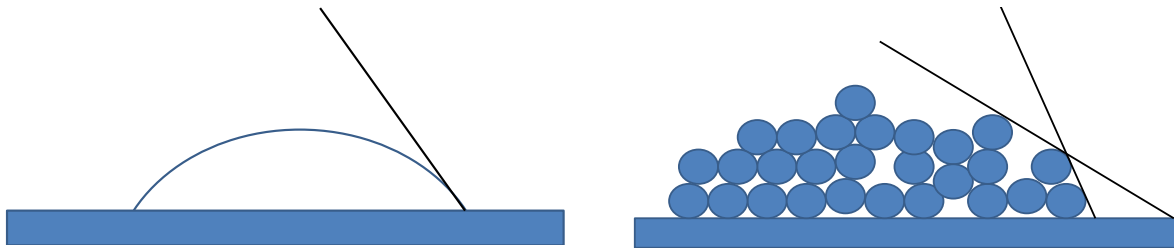
Figure 2.1. Schematics of macroscopic and microscopic droplets to illustrate that the macroscopic contact angle can become difficult to define at the microscopic level (*after Fan and Cagin, 1995*).

surface. The instantaneous contact angle expression is derived from the volume of the droplet and interfacial area between the droplet and the surface, both calculated from the molecular dynamics trajectories. The instantaneous contact angle is calculated for each frame of the trajectories. The contact angle is defined as

$$\cos \theta = 1 - \frac{h}{R} \tag{2.2}$$

where h is the height of the droplet and R is the radius of the sphere.

De Ruijter et al. (1999) used large scale molecular dynamics simulations of droplet spreading to investigate dynamic wetting. In order to calculate contact angles, they defined equilibrium by following the number of liquid atoms in the first surface layer with time. In a system involving 100,480 liquid atoms and 90,000 solid atoms, equilibrium was achieved within 4-5 ns. The layer of liquid in contact with the solid contained about 7% of the liquid atoms. The vapor pressure was assumed to be zero. The density across the liquid-vapor interface was modeled by a sigmoidal function and continuous density profiles were determined at equilibrium by averaging sufficiently over time. In this way, the *equimolar dividing surface* was defined.

The *equimolar dividing surface* was first defined by Gibbs (1961). Gibbs defined the closed surface or interface between two homogeneous phases as a transition region with a finite thickness bounded by planes (Bedeaux and Kjelstrup, 2005). In Figure 2.2A, *a* is a position in gas, and *b* is a position in liquid for a system of one component A. The surface thickness is $\delta = b - a$ for component A. The equimolar dividing surface is a geometrical plane going through points in the interfacial region such that the excess surface concentration in moles of A on one side of the surface is equal to the deficiency of moles of the component on the other side of the surface. In multi-component systems, each component will have an "equimolar" surface. Therefore one component must be chosen as a reference, and the position of the surface is defined as the equimolar dividing surface of the reference component. This component has no excess concentration at the dividing surface, while other components will have an excess
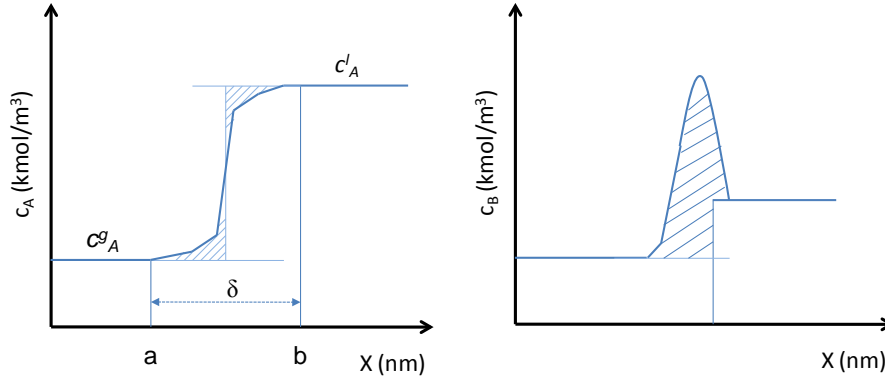
Figure 2.2. Equimolar dividing surface. Concentrations of components A and B are given as C_A and C_B. Concentration of gaseous A is c^g_A and concentration of liquid A is c^l_A.

concentration (see Fig. 2.2B). This will become an important point when calculating contact angles at a material surface between supercritical CO_2 and aqueous solutions.

At equilibrium, the profile of the droplet is a circle. It can deviate from a perfect circle near the solid surface due to liquid-solid interactions. However, on a macroscopic scale, both in theory (i.e., Gibbs' derivation) and in experiment, this deviation is negligible. Therefore, de Ruijter et al. (1999) assumed the contact angle could be determined from a circle extrapolated through the profile, excluding the region influenced by the solid. In their study, the first 10 layers of liquid near the solid surface were excluded from the fitting procedure.

Werder et al. (2003) developed a different technique to calculate contact angles from molecular dynamics simulation trajectories for water droplets on graphite. From the trajectories, water isochore (volume) profiles were obtained by introducing cylindrical binning, which used the top graphite layer as zero reference level and the surface normal through the center of mass of the droplet as reference axis. The bins have a height of 0.5 Å and are of equal volume, i.e., the radial bin boundaries are located at $r_i = \sqrt{i\delta\text{Å}/\Pi}$ for $i = 1, \ldots N_{bin}$ with a base area per bin of $\delta\text{Å} = 95\ \text{Å}^2$. To extract the water contact angle from this profile, a two-step procedure was used. First the location of the equimolar dividing surface was determined within every single horizontal layer of the binned drop. Second, a circular best fit through these points was extrapolated to the graphite surface where the contact angle θ was measured. The points of the equimolar surface below a height of 8 Å from the graphite surface were not taken into account for the fit, to avoid the influence from density fluctuations at the liquid-solid interface. The contact angle depended only weakly ($\sim 1.0^o$) on the elimination of the first few layers of water on the surface. Furthermore only those points for which the density measured in the central bin lies within a range of $0.5 - 1.1\ \text{g/cm}^3$ were used. This effectively excluded the points in the cap region where statistics are poor.

Werder et al. (2003) also accounted for the difference between microscopic and macroscopic contact angles. The macroscopic contact angle (θ_∞) is related to the microscopic

15

contact angle θ through the modified Young's equation developed by Wang et al. (2001) which includes a term to account for the line tension τ or the excess energy associated with the contact line at the boundary between three bulk phases. The line tension plays an important role in determining contact angles for microscopic droplets, the nucleation of droplets on surfaces, and the formation of Newton black films and foam films. It is believed to be significant for droplets with diameters below 10 nm. The effect of a positive line tension is to contract the droplet base and to increase the contact angle whereas a negative τ enhances wetting. The line tension changes sign as temperature increases toward T_w, a first-order wetting transition.

The modified Young's equation relates the surface tensions (γ) to the relevant phases and the line tension (τ) with the contact angle and the droplet base radius r_B as

$$\gamma_{SV} = \gamma_{SL} + \gamma_{LV}cos\theta + \frac{\tau}{r_B} \tag{2.3}$$

Young's equation is recovered for macroscopic droplets, i.e., for $1/r_B \rightarrow 0$. In that case, the macroscopic contact angle θ_∞ is defined as $\cos\theta_\infty = (\gamma_{SV} - \gamma_{SL})/\gamma_{LV}$ and (2) can be rewritten as

$$cos\theta = cos\theta_\infty - \frac{\tau}{\gamma_{LV}}\frac{1}{r_B} \tag{2.4}$$

where the cosine of the microscopic contact angle is linearly related to the droplet base curvature $1/r_B$. A straightforward method to determine the effect of τ in molecular dynamics simulations is to measure the contact angle θ and $1/r_B$ for droplets of different sizes plot $cos\theta$ versus $1/r_B$, and extrapolate to $cos\theta_\infty$.

Daub et al. (2007) adapted the technique developed by Werder et al. (2003) for determining contact angles in an investigation of the sensitivity of water contact angles to applied electric field polarity and direction relative to the water/graphite surface. In the presence of the electric field, the drop can no longer be assumed to be spherical. In an electric field perpendicular to the graphite surface, the vertical drop cross-section is fit to an ellipse instead. In electric fields parallel to the surface, the radial profile is no longer symmetric. The microscopic contact angle is determined by only considering the spheroidal portion of the droplet and by ignoring the first 2-3 layers of water.

Giovambattista et al. (2007) also used a method similar to that described by de Ruijter et al. (1999). They performed molecular dynamics simulations of water in the presence of model walls that ranged in hydrophilicity. For the hydrophilic walls, a hydroxylated silica model was used. This wall was gradually transformed into a hydrophobic surface by modifying the partial atomic charges in the model. In the approach used by Giovambattista et al. (2007), the contact angle was calculated by first defining a z-axis passing through the center of mass of the drop, perpendicular to the solid surface. The drop was then divided into slabs of width 0.5 nm, separated vertically by 0.25 nm, parallel to the surface. For each slab, the density was

determined as a function of drop radius. The drop profile was defined by the slabs in which the horizontal density profile falls to 0.2 g/cm^3. The contact angle was then obtained by fitting curves with the function $r_{\text{drop}}(z) = Az^2 + Bz + C$. The contact angle is given by:

$$\frac{\pi}{2} + tan^{-1}\left(\frac{dr_{drop}}{dz|_{z=0}}\right) \tag{2.5}$$

In this study, we compared the methods of Werder et al. (2003) and Giovambattista et al. (2007) for calculating contact angles on the gibbsite-like and silica surfaces of kaolinite.

3. Computational Methods

3.1. Molecular Model of Kaolinite

Kaolinite ($Al_2Si_2O_5(OH)_4$), a 1:1 clay mineral commonly found in sedimentary basins, is composed of planar sheets of silica tetrahedra and alumina octahedra that coordinate to form a charge-neutral TO (tetrahedron-octahedron) layer (Figure 3.1). The unit cell is triclinic with dimensions a = 5.149 Å, b = 8.934 Å, and c = 7.384 Å and angles $\alpha = 91.93^o$, ß = 105.042^o and γ = 89.791^o. The gibbsite-like surface is hydrophilic with surface hydroxyl groups that readily form numerous hydrogen bonds with overlying water molecules. The silica surface consists of silicon atoms bonded together through bridging oxygen atoms. This surface is more hydrophobic, repelling H_2O molecules. Kaolinite is a good candidate mineral to test our capability to calculate contact angles because it has two surfaces with very different wetting characteristics.

3.2. Simulations

Classical molecular dynamics simulations were used to investigate the formation of water droplets on two kaolinite surfaces. We used the Clayff force field that was developed specifically to examine the interaction of clay minerals with water (Cygan et al., 2004). Clayff consists of an empirically-derived set of interaction parameters to accurately describe the potential energy between atoms in the clay structure. The bonded terms in Clayff are limited to the water molecules and hydroxyl groups within the clay structure and are based on a flexible SPC water model (Berendsen et al., 1981; Teleman et al., 1987).

Simulation cells consist of a water droplet containing 1700 molecules that interacts with a kaolinite surface slab with an exposed surface area 214 Å x 205 Å and a depth of three layers (3 unit cells, 20 Å thickness). The behavior of the water droplets on both the gibbsite-like and silica surfaces of kaolinite was examined. The droplets were placed 10 Å away from either surface in a 180 Å thick vacuum slab. The simulation cell had periodic boundary conditions with box dimensions of 214 Å x 205 Å x 180 Å. Simulation cells were constructed using Materials Studio (Accelyrs, 2009). Prior to setting up simulation cells containing both the kaolinite and water droplets, a 200 ps, NVT simulation of bulk water was used to establish dynamic equilibrium within liquid water with a density of 1 g/cm^3 at 300 K. The water droplet consists of a snapshot from this simulation. Figures 3.2 and 3.3 illustrate the initial simulation cells for the calculations.
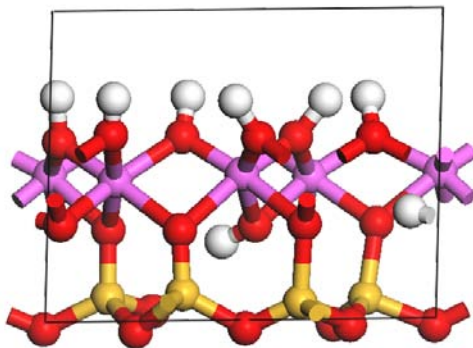
Figure 3.1. Kaolinite unit cell exhibiting a planar sheet of silica tetrahedra overlain by a sheet of alumina octahedra. Al atoms are pink, Si yellow, O red, and H white.

Simulations were carried out using the LAMMPS code (Plimpton, 1995). In some simulations, the kaolinite slab was held completely rigid to expedite the calculations. In other simulations, the kaolinite was held rigid except for the surface hydroxyl groups on the gibbsite-like layer which were allowed to interact with the overlying water droplet. In simulations with a fully flexible kaolinite slab, the kaolinite layers tended to shift with respect to each other and undulate in a non-physical way. In these simulations, the water droplet would migrate with the upper layer of the kaolinite slab, making calculations of the contact angle over time more difficult. Water density profiles for each of these simulations were found to be fairly similar (Figure 3.4), though more of the water molecules were found closer to the surface during the rigid simulations. Previous studies (Werder et al., 2003) have demonstrated that the use of a rigid slab has little to no effect on calculated contact angles, but the computational time is significantly shorter. For each system, a 100 ps equilibration run was performed using an NVE ensemble. Then a 5 ns production run was performed using the canonical ensemble (NVT) with a Nose-Hoover thermostat with a 100 fs time constant to maintain temperature at 300 K. Trajectory data were collected every 2 ps. The data for the last 2 ns, after the water droplet had equilibrated with the kaolinite surface, were used to calculate the contact angles.
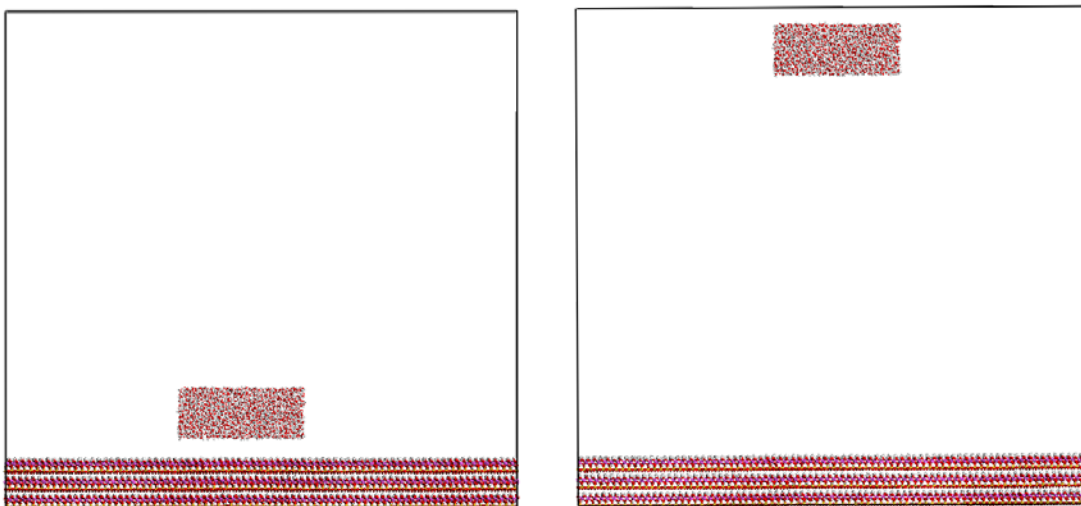
Figure 3.2. Two initial simulation cells to study the formation of a water droplet on the gibbsite-like and silica surfaces of kaolinite. (a) bulk water above gibbsite-like surface, (b) bulk water situated near the silica surface which is located 10 Å away from the base of the simulation cell because of the 3-D periodicity of the calculations.
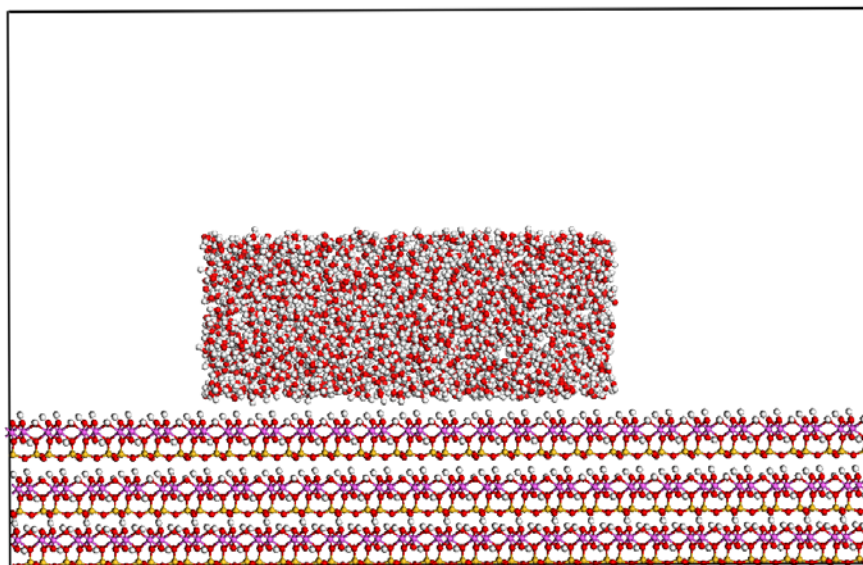
Figure 3.3. An expansion of a section of the simulation cell to more clearly show the hydroxyl groups of the gibbsite-like surface of kaolinite.
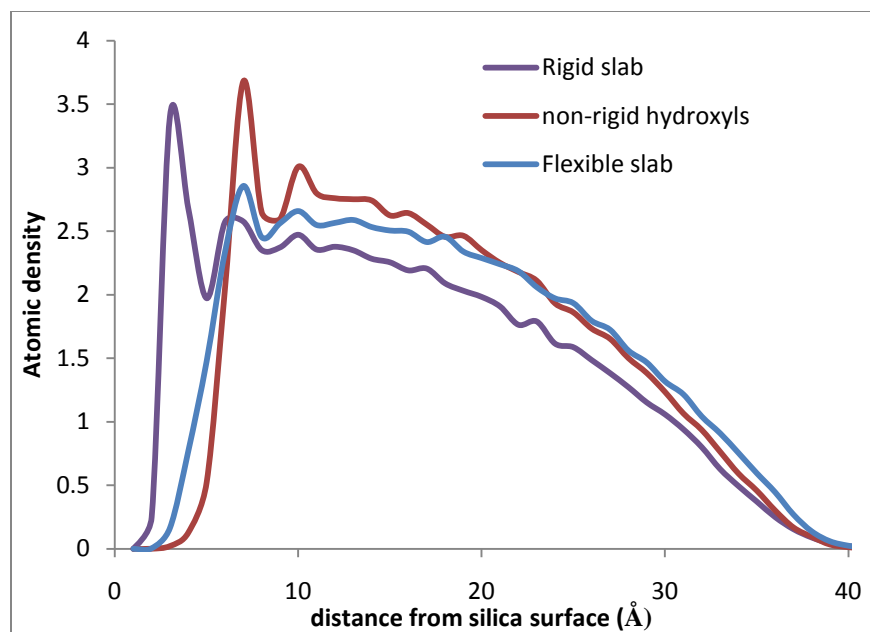
Figure 3.4. Water density profiles (averaged over 100 ps) from simulations for the gibbsite-like surface performed with a rigid kaolinite slab, non-rigid hydroxyl groups on the surface, and a fully-flexible kaolinite slab. After 1 ns, the density profiles for each simulation were constant, indicating the system was likely at equilibrium.

3.3 Contact Angle Calculations

Contact angles were calculated using two approaches: the method described by Werder et al. (2003) and that described by Giovambattista et al. (2007). These approaches were tested by creating MATLAB (Mathworks, 2009) scripts to post-process the molecular dynamics trajectory data. MATLAB was used because it includes curve fitting algorithms, built in plotting functions, and is designed for working with large matrices.

In our application of the Werder et al. (2003) approach, the molecules in the water droplet were distributed into donut-shaped bins with a volume of 95 Å^3. The data on the density of the drop were entered into a histogram. This was done based on the center of mass of the drop, because the drop may move around on the surface over time. The bins are of equal height z and equal area with approximately the same number of molecules. The edge of the drop was defined as the distance in the xy plane from the center of the bin to where the density drops to 50% . This method provides a set of points with equally spaced heights and varying distance d from the central bin. The equimolar dividing surface was calculated to reside in the bins where the water density drops below 50% of the density of bulk water. This surface was taken to represent the liquid-vapor interface. The first 8 Å of water molecules near the kaolinite surface were excluded from the contact angle calculation because these water molecules do not behave like bulk water. The top 5 Å of water molecules were also excluded because of poor statistics in the cap region of the droplet. A circle was fitted to the equimolar dividing surface and extrapolated to the kaolinite surface, where the contact angle was measured. This approach works well for hydrophobic surfaces, but it is difficult to get a reliable circular fit to small arcs characteristic of small contact angles (approx. $< 45^\circ$; Daub, *pers. comm.*).

Because we want to be able to calculate contact angles for both hydrophobic and hydrophilic surfaces, we also adapted the method developed by Giovambattista, et al. (2007). The water drop was divided into slabs of width 1 nm and height .25 nm. We chose to use a width larger than that used in Giovambattista et al. (2007) because of the considerable spread of the drop on the gibbsite-like surface. We divided the slabs into bins of length 0.2 nm and determined the number of water molecules that would be found in each of those bins. More information on how these dimensions were chosen can be found in the discussion. Then, the radius from the z-center of mass of the drop was calculated for the bins in which the water density dropped below 0.2 g/cm^3. These points were used to define the drop profile or the equimolar dividing surface. The drop profile was fit with a 2nd degree polynomial or a spline function. Only drop radii larger than 1.5 nm were included in the fit, which eliminated the cap region of the droplet. The contact angle was calculated using Equation 2.5.

In both of these methods the contact angle calculated is defined to be the microscopic contact angle. This is related to the macroscopic contact angle by Equation 2.3. The line tension for water has previously been calculated to be on the order of 10^{-10} J/m, and should only be

significant for droplets smaller than 10 nm in diameter. Our drops have diameters of approximately 5 nm (for the silica surface) and 14 nm (for the gibbsite-like surface); however, results from the literature only report the microscope contact angle, therefore we did not consider line tension in our contact angle calculations.

Calculate Bins for Water Droplet

0.5 Å

$r_1+r_2+r_3$

Axis through **R**
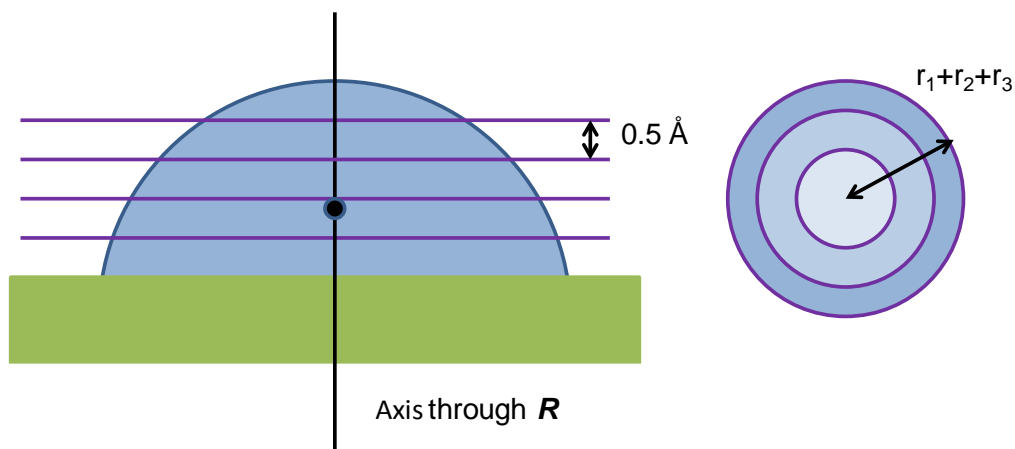
Calculate Center of Mass for Droplet

$$R = \frac{\sum m_i r_i}{\sum m_i}$$

R = Center of mass
m_i = Mass of particle
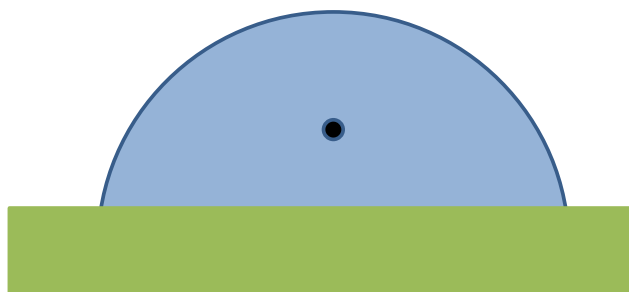**r_i** = Position of the
        ith particle

Figure 3.5. Illustration of binning according to Werder et al. (2003).

4. Results and Discussion

Calculating contact angles correctly from molecular dynamics simulations will be a valuable tool to study the interaction of supercritical CO_2 with water and different mineral substrates in the geological environment. However, comparisons are necessary between experimentally determined contact angles and our computations to ensure that our results are accurate. Contact angles of aluminosilicate clays are difficult to determine because they may vary with relative humidity and exchangeable cations. In addition, clays typically have small particle sizes that present measurement difficulties (Shang et al., 2010). Shang et al. (2008) compared five different experimental methods to determine contact angles on smectite, kaolinite, illite, goethite, and hematite. In Shang et al. (2010), contact angles for Arizona smectite (SAz-1), Georgia kaolinite (KGa-1b), and illite (Morris No. 36) were measured under different conditions. The clays were fractionated to obtain particles smaller than 2 µm in diameter. Two types of size-fractionated (< 2 um) clays were used in their experiments: (1) non-treated clays as obtained from the supplier, and (2) clays saturated with Na, K, Mg, or Ca; dialyzed to 1 µS/cm; and pretreated to remove organic matter, Fe, and acid-soluble impurities. Static contact angles were determined with the sessile drop method. For kaolinite, Shang et al. (2010) measured contact angles between 17.3^o and 20.6^o at four different humidities ranging from 19% - 100%, with no trend associated with relative humidity. The lowest contact angle 17.3^o was found for 100% relative humidity. Contact angles for non-treated kaolinite and kaolinite samples saturated with Ca, Na, K, or Mg were measured to be roughly the same, ranging from 16.9^o to 17.5^o. In all cases, the contact angles measured are for the adsorption of water on the gibbsite-like surface of clay.

No contact angle measurements for the silica surface of clay were found in the literature. However, Chai et al. (2009) investigated the microscopic wetting of water on amorphous silica surfaces using molecular dynamics and found that hydrophobicity becomes enhances with an increase in surface silanization. For surfaces with >70% surface coverage with $-Si(CH_3)_3$ groups, the water contact angle remains unchanged at between $110-120^o$. This contact angle is the microscopic contact angle as the authors did not account for the tension associated with smaller drops.

Using Giovambattista et al.'s (2007) methods, we calculated contact angles for the silica surface and gibbsite-like surface of kaolinite of 110° and 12° respectively. These angles are fairly dependent on the bin dimensions chosen. Table 4.1 and Figure 4.1 show a comparison of varying bin dimensions and the corresponding effect on the contact angle for the silica surface. The largest contact angle (120˚), calculated in Trial 2, appears to underestimate the drop size (see Figure 4.1) and the location of the dividing surface, suggesting the bin size used, $20\mathring{A}^3$ is too small. The smallest contact angle, 105˚, is also calculated using a bin size of $20\mathring{A}^3$ (Trial 6). This suggests that bin sizes closer to $50\mathring{A}^3$ (Trials 3 and 4) are better for reproducing the dividing

surface. However, increasing the bin size too much decreases the resolution to a point where an accurate dividing surface cannot be calculated.

Figure 4.2 illustrates the impact of including the cap region of the droplet on the overall fit to the equimolar dividing surface for the silica surface. The cap region of the droplet is characterized by poor sampling statistics. Including this region leads to a poor fit to the dividing surface and a dramatically different contact angle determination.

Our calculation of a contact angle of 110° (Trial 3) for the silica surface using the method of Giovambattista et al. (2007) compares well with the simulation results of Chai et al. (2009). We also calculated this contact angle using the Werder et al. (2003) method and found a contact angle of 115°, and the Fan and Cagin (1995) method which gave a contact angle of 113°. However, we were not able to calculate a contact angle using the Werder et al. (2003) method for the gibbsite-like surface because fitting a circle to such a small angle is very inaccurate, and the Fan and Cagin (1995) method appeared to underestimate the contact angle at 7°. The Giovambattista et al. (2007) method yielded a contact angle of 12.6^o on the gibbsite-like surface, which is still lower than the experimentally measured angles of 17.3^o and 20.6^o (Shang et al., 2010). However, Shang et al. (2010) suggest that experimentally distinguishing between measured contact angles less than 20° is difficult. Therefore, we conclude that the method of Giovambattista et al. (2007) is the best to date to calculate contact angles on both hydrophobic and hydrophilic surfaces.

The accuracy of all these methods will improve with larger water drops and simulation cells as well as the collection of trajectory data over longer time periods. Comparisons with experimentally- determined contact angles on different surfaces should be made as these measurements become available. Confirmation that this method can be used successfully to calculate contact angles on kaolinite suggests that now contact angles involving more complex systems can be studied. These systems might include the interfaces between different phases of CO_2 or organic fluids with silicate minerals including quartz, feldspars, mica, and more complex clay minerals such as montmorillonite and pyrophyllite, all of which make up significant portions of sedimentary basins. In addition, this approach may be extended to calculate contact angles between two fluids (e.g., supercritical CO_2 and H_2O), establish the relative wettability of different mineral surfaces to these fluids, and examine fluid mixing at these surfaces.

Table 4.1. Comparison of calculated contact angles for silica surface using Giovambattista et al.'s (2007) method based on different bin sizes.

Trial	contact angle	dx (Å)	dy (Å)	dz (Å)	Volume (Å^3)
1	117.75	1	10	2.5	25
2	120.02	1	10	2	20
3	110.35	2	10	2.5	50
4	115.76	2	10	2	40
5	111.96	2	5	2.5	25
6	105.65	2	5	2	20

Trial 1
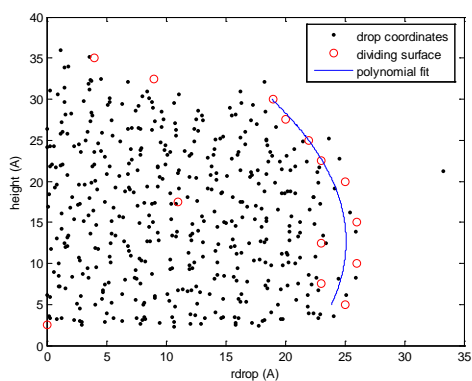
Trial 2
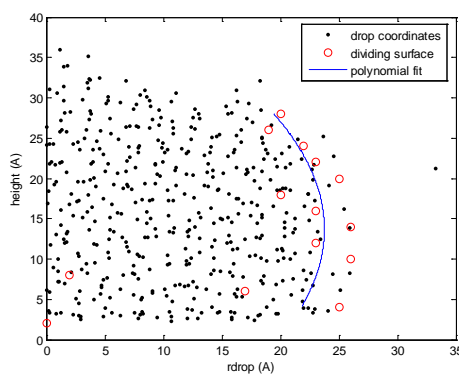
Trial 3
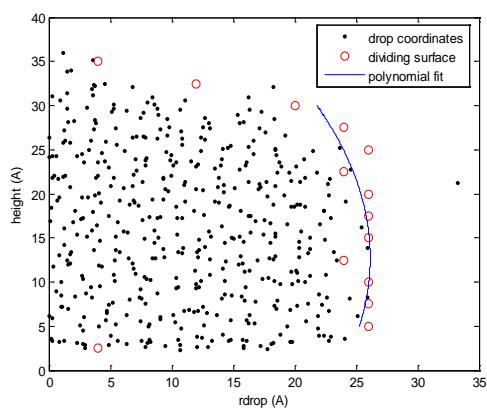
Trial 4

Trial 5
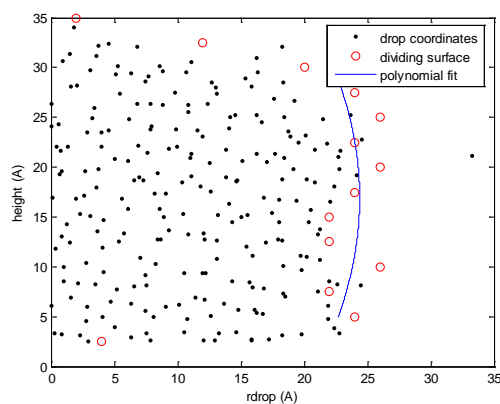
Trial 6
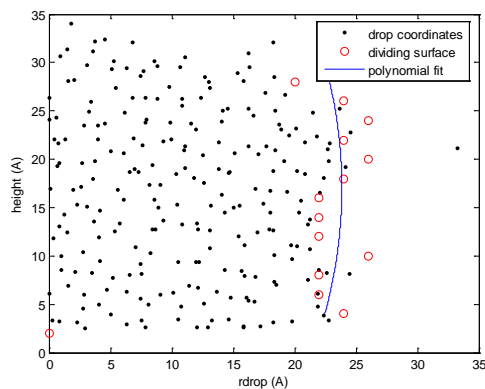
Figure 4.1. Comparison of polynomial fits to the equimolar dividing surface for the silica surface using different bin dimensions. Bin dimensio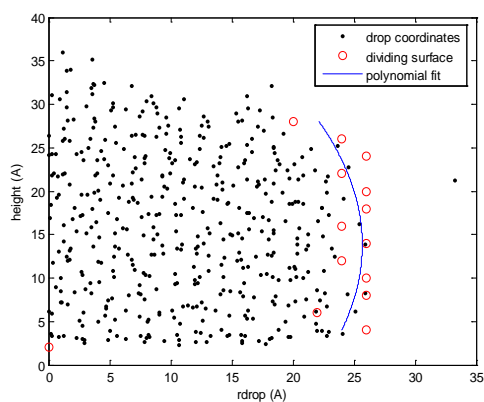ns for each trial are provided in Table 4.1. Trial 3 provides the best fit to the dividing surface and yields a contact angle of 110°.
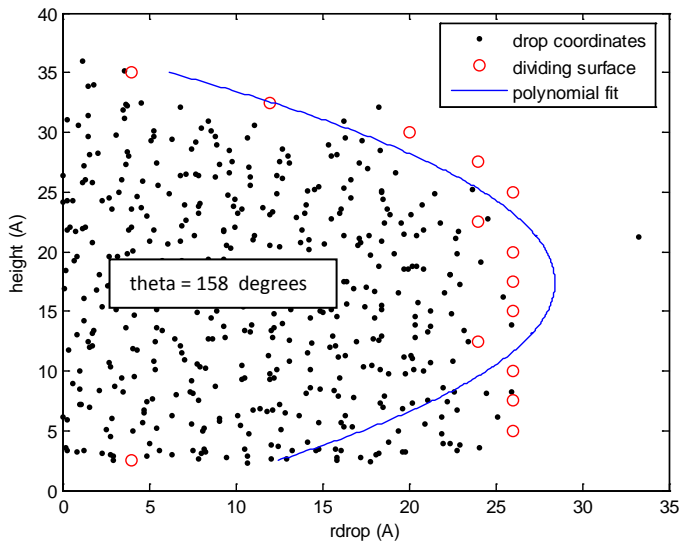
**Figure 4.2. Calculation the contact angle on the silica surface with the cap region
included in fitting the dividing surface.** Including the cap region led to a calculated contact
angle of 158°, and an extremely poor fit to the dividing surface, showing that exclusion of the
cap region is necessary for these calculations due to poor sampling statistics in that region.
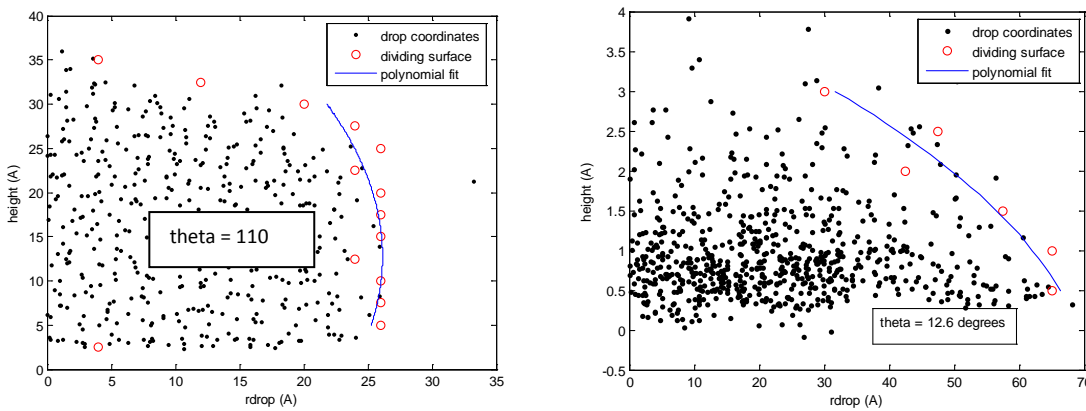
**Figure 4.3. The liquid/vapor interface fit to the calculated dividing surface for a drop on
the (A) silica surface and (B) gibbsite-like surface.** In (A), the contact angle is 110°,
indicating wetting is not favorable for the silica surface. In (B) the contact angle is 12.6°,
indicating wetting is favorable for the gibbsite-like surface.

5. References

Accelyrs. (2009) Materials Studio Software. Accelyrs, Inc., San Diego.

Bedeaux, D. and S. Kjelstrup (2005) Heat, Mass and Charge Transport, and Chemical Reactions at Surfaces. *International Journal of Thermodynamics*, *8*, 25-41.

Berendsen, H. J. C., J. P. M. Postma, W. F. van Gunsteren, and J. Hermans (1981), Interaction models for water in relation to protein hydration, in *Intermolecular Forces*, edited by B. Pullman, pp. 331-342, D. Reidel.

Chai, J., S. Liu, and X. Yang (2009), Molecular dynamics simulation of wetting on modified amorphous silica surface, *Applied Surface Science*, *255*, 9078-9084.

Cygan, R. T., J.-J. Liang, and A. G. Kalinichev (2004), Molecular Models of Hydroxide, Oxyhydroxide, and Clay Phases and the Development of a General Forcefield, *Journal of Physical Chemistry B*, *108*, 1255-1266.

Daub, C. D., D. Bratko, K. Leung, and A. Luzar (2007), Electrowetting at the Nanoscale, *The Journal of Physical Chemistry C*, *111*, 505-509.

de Ruijter, M. J., T. D. Blake, and J. De Coninck (1999), Dynamic wetting studied by molecular modeling simulations of droplet spreading, *Langmuir*, *15*, 7836-7847.

Fan, C. F., and T. Cagin (1995), Wetting of crystalline polymer surfaces: A molecular dynamics simulation, *Journal of Chemical Physics*, *103*, 9053-9061.

Giovambattista, N., P. G. Debenedetti, and P. J. Rossky (2007), Effect of surface polarity on water contact angle and interfacial hydration structure, *Journal of Physical Chemistry B*, *111*, 9581-9587.

Hautman, J., and M. L. Klein (1991), Microscopic Wetting Phenomena, *Physical Review Letters*, *67*, 1763-1766.

Israelachvili, J. (1992), Intermolecular and Surface Forces, Academic Press, London. 450pp.

Mathworks. (2009) MATLAB

Plimpton, S. (1995), Fast Parallel Algorithms for Short-Range Molecular Dynamics, *Journal of Computational Physics*, *117*(1), 1-19.

Shang, J., M. Flury, J. B. Harsh, and R. L. Zollars (2008), Comparison of different methods to measure contact angles of soil colloids, *Journal of Colloid and Interface Science*, *328*.

Shang, J., M. Flury, J. B. Harsh, and R. L. Zollars (2010), Contact angles of aluminosilicate clays aas affected by relative humidity and exchangeable cations, *Colloids and Surfaces A: Physicochemical and Engineering Aspects*, *353*, 1-9.

Teleman, O., B. Jonsson, and S. Engstrom (1987), A molecular dynamics simulation of a water model with intramolecular degrees of freedom, *Molecular Physics*, *60*, 193-203.

Wang, J. Y., S. Betelu, and B. M. Law (2001), Line tension approaching a first-order wetting transition: Experimental results from contact angle measurements, *Physical Review E, 63,* Article #031601, 11p.

Werder, T., J. H. Walther, R. L. Jaffe, T. Halicioglu, and P. Koumoutsakos (2003), On the Water-Carbon Interaction for Use in Molecular Dynamics Simulations of Graphite and Carbon Nanotubes, *Journal of Physical Chemistry B*, *107*, 1345-1352.

6. Appendix 1

MATLAB SCRIPT FOR GIOVAMBATTISTA ET AL. (2007)

```
function [theta, xdens] = binning_Gbassti(filename, zbin, xbin, dx, dy, dz)

%function needs to be given a filename, the number of bins in the x and
%z directions, and the size of the bin in the x, y, and z directions

%zbin should be approximately equal to the height of the drop/dz
%xbin should be approximately equal to the length of the drop/dx
%dx, dz should be small (<5 A)
%dy should be greater than dx, dz

%%%Filename format: (.lammpstrj format)
% 1st col = atom number
% 2nd col = atom type
% 3rd col = x position
% 4th col = y position
% 5th col = z position
%%%

%%constants:
avagadrosNum = 6.022*10^23;
massH = 1.008; massO = 15.999;
massOfWater = 2*massH+massO;
zlength = 200; xlength =205; ylength = 214;

%%creating some variables of interest
hist = zeros(zbin,xbin); a = zeros(zbin,xbin);
H = zeros(1, zbin); G = zeros(1, xbin); dens = zeros(1, round(zbin/dz));

%%load the file
water = filename;
water = sortrows(water,1);  %sorting by atom number

%%extract all the waters and convert to position
j = 0;
for i = 1:103020
    if water(i,2) >= 6        %atom type greater than 5 was the fluid
                              %for our simulations
        j = j + 1;
        water2(j, 1:5) = water(i,1:5);
    end
end

x = water2(:,3)*xlength;
y = water2(:,4)*ylength;
z = (1- water2(:,5))*zlength;

%%get rid of most molecules not in x/y/z_drop
j = 0;
for i = 1:length(x)
```

```
      if z(i) <= zlength/2
         j = j+1;
         z_drop(j) = z(i);
         y_drop(j) = y(i);
         x_drop(j) = x(i);
      end
   end
x = x_drop; y = y_drop; z = z_drop;

%%find center of mass of each molecule
for i = 1:length(x)/3
   xcm(i) = (x(i*3)*massH+x(i*3-1)*massH+x(i*3-2)*massO)/massOfWater;
   ycm(i) = (y(i*3)*massH+y(i*3-1)*massH+y(i*3-2)*massO)/massOfWater;
   zcm(i) = (z(i*3)*massH+z(i*3-1)*massH+z(i*3-2)*massO)/massOfWater;
end

%%Find center of mass of drop
cmx = sum(xcm)/length(x)*3;
cmy = sum(ycm)/length(y)*3;
cmz = sum(zcm)/length(z)*3;

%%creating a slab to find the dividing surface
j = 0;
for i = 1:length(xcm)
   if ycm(i) <= (dy+cmy) && ycm(i) >= (cmy-dy)   %if y value for this molecule is in range of interest
      if xcm(i) <= cmx                           %divides the drop in half in the x direction
         j = j+1;
         xslab(j) = cmx - xcm(i);
         zslab(j) = zcm(i);
      end
   end
end

for i = 1:zbin
   H(i) = i*dz;
end

for i = 1:xbin
   G(i) = i*dx;
end

%%binning
hist = zeros(zbin,xbin); a = zeros(zbin,xbin);
for i = 1:length(xslab) %for each molecule in slab
   zflag =0; xflag=0; k=0; l= 0;
   %find the z range it is a member of with resolution of dz
   while zflag == 0
      k = k+1;
      if zslab(i) <= H(k)
         zflag = 1;
      end
      if k == 1
      end
      if k == round(zbin)
         zflag = 1;
      end
   end
```

34

```
        end


    %find the x range it is a member of with resolution of dx
    while xflag == 0
        l = l+1;
        if xslab(i) <= G(l)
            xflag = 1;
        end
        if l == 1
        end
        if l == round(xbin)
            xflag = 1;
        end
    end

    hist(k,l) = hist(k,l)+1;                              %hist counts number of molecules in each bin
    massBin = hist(k,l)/avagadrosNum*massOfWater;        %mass in grams
    volBin = (dx*dz*dy*(1e-8)^3);                        %volume in cm^3
    a(k,l) = massBin/volBin;                              %calculate density for the current bin
end

%%determining the dividing surface
for k = 1:floor(zbin)   % for each zbin
    rflag = 0;
    l = 1;
    while rflag ~= 1
        if 1/2*(a(k,l)+a(k,l+1)) <= .2         %if average density of this two consecutive xbins
                                               %in the same zbin is less than .2 g/L
            rflag = 1;                         %set flag
        else
            l = l + 1;
            if l+1 >= xbin              %if last xbin
                rflag = 1;             %set flag
            end
        end
        dens(k) = l-1;                 %counts number of bins that pass the test, for each zbin
                                       %(gives a matrix)
    end
end

%Fitting

dens = dens*dx;                     %converts the number of bins to a distance (dividing surface)
range = dz:dz:zbin*dz;
range2 = (1:length(range));
XY = [(dens(range2))', (range)'];
j = 0;
for i = 1:length(range)
    if XY(i, 1) > 15   %excludes top of drop
        j = j + 1;
        xdens(j, :) = XY(i,:);
    end
end
```

```
xx = min(xdens(:,2)):.1:max(xdens(:,2));
p = polyfit(xdens(:,2), xdens(:,1), 2);              %fits to a polynomial of degree 2
yfit = polyval(p, xx);                               %uses the fit to calculate the radius



%plotting
figure
plot(xslab, zslab,'k.')                               %plots all the molecules in the slab of interest
hold on
plot(dens(range2), range, 'ro')          %plots dividing surface
hold on
plot(yfit, xx, 'b')                      %plots the fit
hold off

theta = (pi/2 + atan(p(2)))*180/pi;       %angle calculated from method described
                                          %in: Giovambattista, et al. (2007)
xlabel('rdrop (A)')
ylabel('height (A)')
legend('drop coordinates', 'dividing surface', 'polynomial fit')
```

7. Distribution

1	MS0359	D. Chavez, LDRD Office	1911
1	MS0899	Technical Library	9536 (electronic copy)